

# THE INFLUENCE OF MICROSTRUCTURE ON THE CORROSION PROPERTIES OF Cu POLYCRYSTALS PREPARED BY ECAP

MILOŠ JANEČEK<sup>1\*</sup>, BRANISLAV HADZIMA<sup>2</sup>, RALPH JÖRG HELLMIG<sup>3</sup>,  
YURI ESTRIN<sup>3</sup>

<sup>1</sup>*Charles University, Faculty of Mathematics and Physics, Department of Metal Physics,  
Ke Karlovu 5, CZ-121 16 Prague 2, Czech Republic*

<sup>2</sup>*University of Žilina, Faculty of Mechanical Engineering, Univerzitná 1, SK-010 26  
Žilina, Slovak Republic*

<sup>3</sup>*Clausthal University of Technology, Institute of Material Science and Engineering,  
Agricolastr. 6, D-38678 Clausthal-Zellerfeld, Germany*

Received 14 February 2005, accepted 7 June 2005

Submicrocrystalline and/or nanocrystalline materials prepared by severe plastic deformation possess improved properties as compared to their coarse grained (CG) counterparts. Ultra-fine grained (UFG) copper polycrystals prepared by equal channel angular pressing (ECAP) to various strain (1, 2, 4 and 8 passes) were investigated. ECAP processing resulted in grain size reduction by a factor of about 100. TEM analysis showed that the original CG microstructure evolves from prolate bands of cells/subgrains enclosed by lamellar nonequilibrium grain boundaries towards a more equiaxed homogeneous microstructure with equilibrium grain boundaries. The influence of the microstructure on the corrosion properties in three different aggressive media, viz. 3% NaCl, 1M HCl and the standard Livingston solution was investigated by conventional potentiodynamic polarization measurements. While the general corrosion characteristics are almost unaffected by grain refinement, the corrosion damage is more homogeneous in the UFG material, which contrasts clearly localized intergranular corrosion in CG material. This is a promising property of UFG material for engineering applications.

**Key words:** UFG copper, ECAP, microstructure evolution, corrosion behaviour

---

\*corresponding author, e-mail: janecek@met.mff.cuni.cz

## 1. Introduction

Equal channel angular pressing (ECAP) has been identified as an efficient method of obtaining submicrocrystalline (grain size  $d < 1 \mu\text{m}$ ) and/or nanocrystalline grain sizes ( $d < 100 \text{ nm}$ ) in bulk metallic materials. It allows a repetitive pressing of a billet through a die having two intersecting channels without changing its cross-sectional dimensions. Very high shear strains can therefore be produced. The ultra-fine grained structures exhibit a number of beneficial properties as compared with coarse grained crystals. Recent investigations of UFG materials have concentrated mainly on structural characterization [1–3], microhardness variation [4, 5], mechanical properties [6, 7], elastic and damping properties [8], fatigue [9] and creep [10]. Several models have been also developed to relate the mechanical properties of UFG metals to the evolution of the microstructure and texture [11, 12]. By contrast, corrosion behaviour of UFG materials has received only limited attention. The first literature reports were ambiguous. While Aust et al. [13] showed that nanostructured materials may possess improved corrosion properties as compared to coarse grained polycrystals, some other authors reported significant degradation of corrosion resistance in nanocrystalline state [14]. These contradictory reports make it difficult to predict corrosion behaviour of a given material based on known properties of its coarse-grained state. Therefore a systematic study and characterization of corrosion behaviour of UFG materials is important both for better understanding of their fundamental physical properties and for their possible engineering applications. Pure copper is a suitable candidate for these studies as the corrosion behaviour of coarse grained polycrystals has been studied extensively [15, 16] and bulk UFG copper can be relatively easily produced by severe plastic deformation.

## 2. Experimental

Technical purity (99.95 %) Cu was severely deformed by equal channel angular pressing (ECAP) to a maximum equivalent strain of 8 (1, 2, 4 and 8 passes) at room temperature following route B<sub>c</sub>. Prior to ECAP processing the specimens were annealed for 2 hours at 450 °C in a protective inert atmosphere. The initial specimen dimensions were 10 mm × 10 mm × 60 mm.

The ECAP die used was manufactured from a common tool steel (X38 CrMoV 51). After machining, the die was hardened to 47 HRC. The die has a split design where one part contains the full channel and the other part is used for die closure. The angle  $\Theta$  between two intersecting channels and the corner angle  $\Psi$  are 90° and 0°, respectively. Both channels have a square cross section of 10 mm × 10 mm. The length of the exit channel was optimized to allow easier processing while maintaining the straight shape of the specimen on exit. The die was placed in a hydraulic INSTRON 8502 machine which allows a maximum applicable load

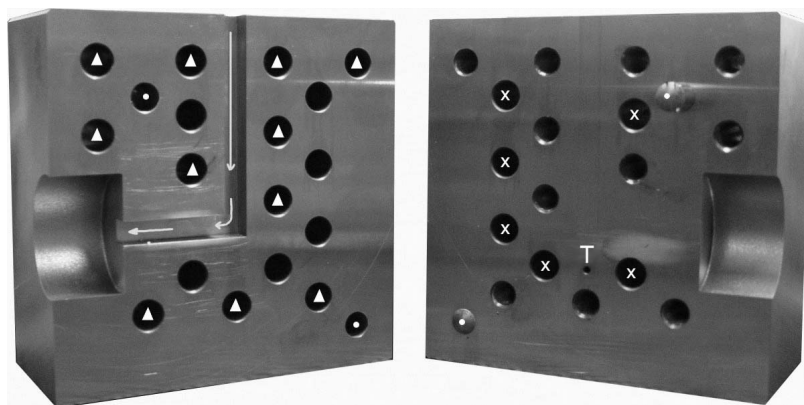


Fig. 1. ECAP die used in the experiments reported.

of 200 kN. Pressing was performed with the speed of 8 mm/min and molybdenum disulphide grease was used as a lubricant. A photograph of the die is shown in Fig. 1. (The dots indicate the positioning pins, the crosses the positions of heating elements and the triangles the positions of fastening bolts; T designates the position of a thermocouple.)

Transmission electron microscopy investigations were performed with a Philips CM 200 electron microscope operated at 200 kV. Specimens for TEM were mechanically cut from the uniformly deformed middle sections of ECAP processed specimens normal to the extrusion direction. The specimens were first mechanically polished and then electropolished in Tenupol 5 double jet polishing unit in the 50%  $\text{H}_3\text{PO}_4$  solution with water at 10 °C.

Corrosion measurements were carried out using a conventional three-electrode device Voltalab 10 – PGZ 100 (Radiometer Analytical SAS, France). A saturated calomel electrode (SCE) with a Luggin capillary was used as a reference electrode, while a Pt plate served as the counter electrode. The working electrode (the test specimen) was insulated with Teflon in the cell wall so that the exposed area was approximately 20 mm<sup>2</sup>. All potentials are referred to the SCE reference electrode. The details of this experimental unit are described elsewhere [17].

Before the measurements samples were mechanically polished on fine emery papers and then electropolished in the solution of 70 ml  $\text{H}_3\text{PO}_4$  and 30 ml  $\text{CH}_3\text{COOH}$  to reduce the surface damaged layer and to obtain the mirror-like surface. 1M HCl, 3% NaCl with double distilled water and the standard Livingston etchant [18] (30 ml HCl + 10 ml  $\text{CH}_3\text{COOH}$  + 410 ml  $\text{H}_2\text{O}$ ) were used as test solutions. All measurements were performed at room temperature. Upon immersion, the specimens were kept in the test solution for 10 minutes, in order for them to attain a

steady state open-circuit potential. The specimens were first cathodically charged at a potential of  $-200 \text{ mV}_{\text{SCE}}$  to remove any oxide films which may have formed on the surface. Each potentiodynamic curve was obtained by potential sweeps of  $1 \text{ mV} \cdot \text{s}^{-1}$  starting from  $-200 \text{ mV}_{\text{SCE}}$  and terminating usually at a transpassive potential of  $800 \text{ mV}_{\text{SCE}}$ . Corrosion potential  $E_{\text{corr}}$  and the corrosion current density  $i_{\text{corr}}$  were evaluated from the individual potentiodynamic curves using the Tafel extrapolation procedure [17].

The microstructure of the initial state was examined by scanning electron microscopy using a Tesla BS343 SEM microscope operated at 15 kV.

### 3. Experimental results

#### 3.1 Microstructure evolution during ECAP

A SEM micrograph of the initial state before ECAP pressing is shown in Fig. 2. The microstructure consists of fully recrystallized grains. Extensive twinning associated with annealing at  $450^\circ\text{C}$  is also seen. The average grain size excluding twins is approximately  $30 \mu\text{m}$ . Bright field TEM micrographs showing the development of the microstructure oriented along  $\langle 011 \rangle$  zone axis are presented in Fig. 3. After 1 pass (Fig. 3a) the microstructure mainly consists of strongly elongated dislocation cells and/or subgrains of average cross-sectional size of  $300\text{--}400 \text{ nm}$ . Two types of boundaries can be recognized in this micrograph. The thick dark lines can be identified as lamellae boundaries [3] or dense dislocation walls (DDW) [18] while the lighter and wider ones are individual dislocation cell boundaries. The DDWs usually enclose several cells and are classified as geometrically necessary boundaries as they are necessary to accommodate lattice rotations in adjoining volume. Selected area diffraction observations showed that these boundaries are mainly low angle ones and are oriented along the trace of a  $\{111\}$  plane, which indicates that they are parallel to a  $\langle 110 \rangle$  shear direction. They are in a nonequilibrium state as they contain a high density of extrinsic dislocations. In some regions (approximately 20 % of the area investigated) a tangled dislocation structure, which is typical of heavily deformed material, was observed.

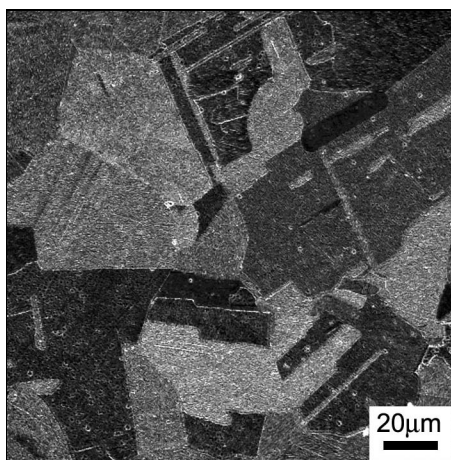


Fig. 2. SEM micrograph of the coarse grained Cu (etchant:  $2 \text{ g K}_2\text{Cr}_2\text{O}_7 + 100 \text{ ml dist. H}_2\text{O} + 4 \text{ ml sat. NaCl} + 8 \text{ ml H}_2\text{SO}_4$ ).

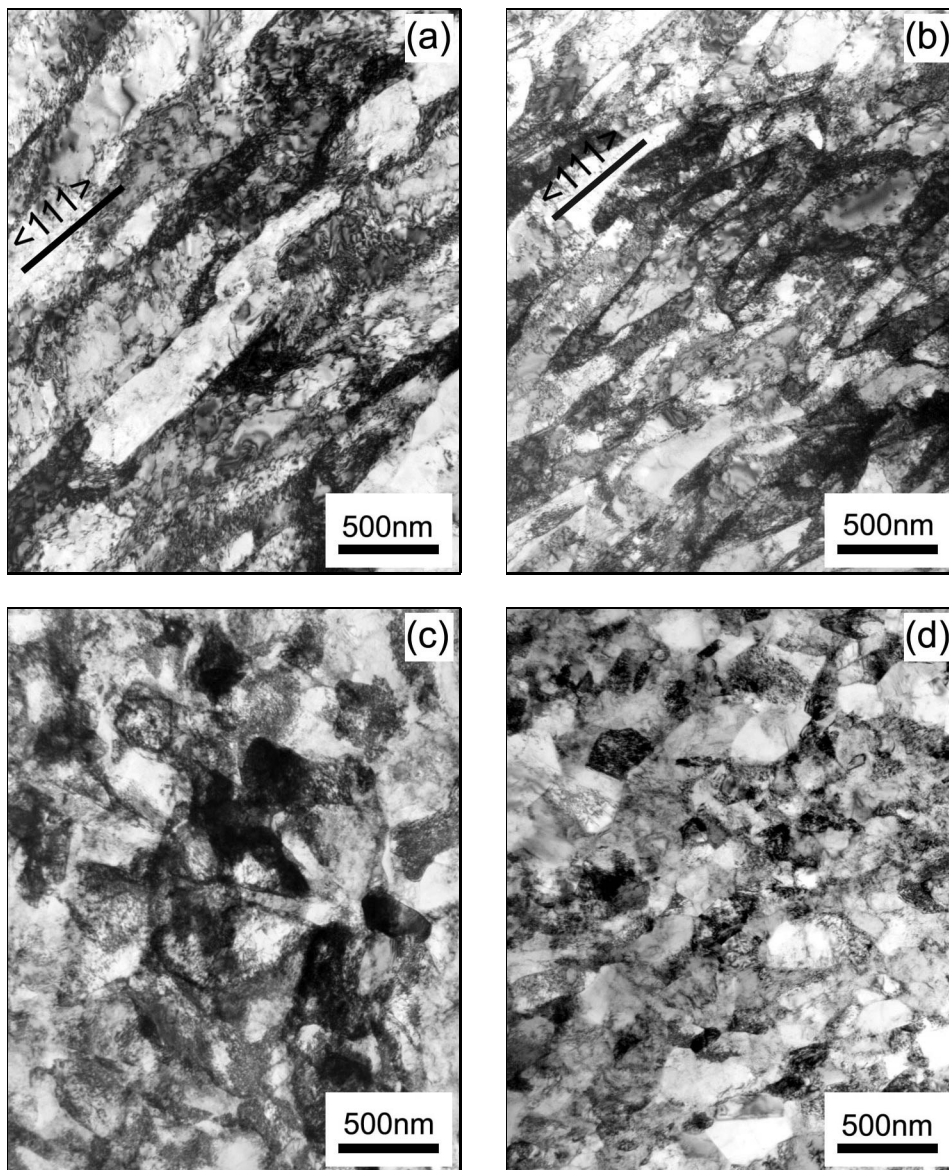


Fig. 3. Bright field TEM micrographs of microstructure evolution of Cu processed by a) 1 pass, b) 2 passes, c) 4 passes and d) 8 passes of ECAP.

After the second pass (Fig. 3b) the microstructure did not change significantly. Bands of elongated subgrains were found in all areas of the specimen.

The average size of individual boundaries slightly decreased to 200–300  $\mu\text{m}$ . Most of the boundaries were still aligned along the trace of a  $\{111\}$  plane. In a few areas lamellae boundaries oriented along a  $\{220\}$  plane trace were also observed. More equiaxed subgrains with higher misorientation indicating the activity of additional slip systems during the second pass were also found locally.

After four passes (Fig. 3c) the fraction of equiaxed subgrains increased and the larger proportion of high angle grain boundaries was observed in the structure. Equiaxed grain structure was found approximately in 40–50 % of the observed area. This is an indication that many new slip systems which are not parallel to the original slip system became active between the second and fourth pass of pressing reducing the length of the original subgrain boundaries.

The microstructure of the specimen after 8 passes is presented in Fig. 3d. It shows an almost homogeneous microstructure with equiaxed subgrains separated mostly by high angle grain boundaries. The individual boundaries are straight with sharp contrast and very few dislocations in the grain interior. They are obviously closer to the equilibrium state than grain boundaries in the specimens that underwent a smaller number of ECAP passes. The average grain size ranged between 200–300 nm. In some areas bigger grains having the average size of about 500 nm were also found.

### 3.2 Corrosion behaviour of UFG Cu

The individual electrochemical characteristics of UFG Cu were determined using potentiodynamic measurements and compared with those of a coarse grained Cu polycrystal. Two test solutions with  $\text{Cl}^-$  ions differing in pH value were used, namely 1M HCl (pH = 0.16, 35.453 g of  $\text{Cl}^-$  in 1 liter of solution) and 3% NaCl (pH = 7.01, 18.199 g of  $\text{Cl}^-$  in 1 liter of solution) with double distilled water. Standard Livingston solution (pH = 0.46) was also used to compare our results with those obtained by other authors [19].

The following corrosion characteristics were evaluated from the potentiodynamic curves:

- the corrosion potential  $E_{\text{corr}}$  – a thermodynamic characteristic of the material surface in a corrosion environment that is a measure of its corrosion resistance,
- the corrosion current density  $i_{\text{corr}}$  which characterizes the rate of corrosion in a given medium at the corrosion potential  $E_{\text{corr}}$ ,
- the steady state anodic current density  $i_{\text{an}}$  which is achieved after surface passivation and characterizes the dissolution rate in the passive state and
- the active-passive transition potential  $E_p$  (or  $E_{p1}, E_{p2} \dots E_{pn}$  in case of  $n$  active-passive transitions) at which a passive protective layer is created on the specimen surface.

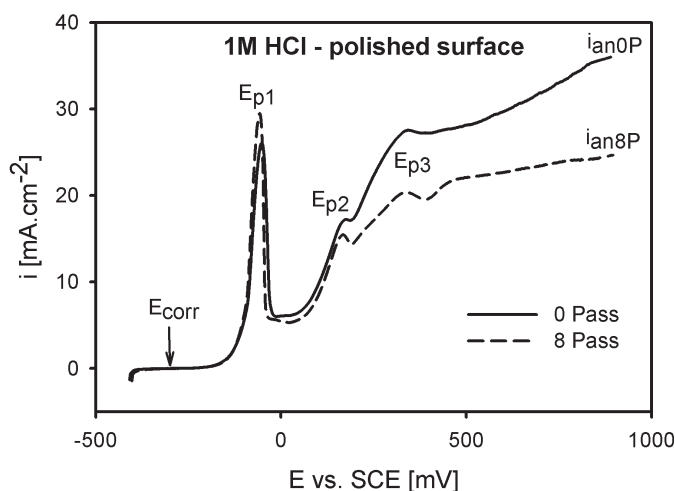


Fig. 4. Potentiodynamic polarization curves of a coarse grained Cu (0 Pass) and ultra-fine grained Cu (8 Passes) in 1M HCl solution.

Table 1. Corrosion characteristics of coarse grained and ultra-fine grained copper in three aggressive solutions (P – electrolytically polished surface, R – ‘rough’ mechanically polished surface)

1M HCl		$E_{\text{corr}}$ [mV]	$i_{\text{corr}}$ [ $\mu\text{A}/\text{cm}^2$ ]	$i_{\text{an}}$ [ $\text{mA}/\text{cm}^2$ ]	$E_{\text{p1}}/E_{\text{p2}}/E_{\text{p3}}$ [mV]
0 Pass	P	-282	13	34*	-50/180/346
	R	-200	300	23	-65/175/352
8 Passes	P	-275	13	24	-56/174/348
	R	-183	317	28	-59/167/373
3% NaCl		$E_{\text{corr}}$ [mV]	$i_{\text{corr}}$ [ $\mu\text{A}/\text{cm}^2$ ]	$i_{\text{an}}$ [ $\text{mA}/\text{cm}^2$ ]	$E_{\text{p1}}/E_{\text{p2}}$ [mV]
0 Pass	P	-234	23	12*	37/195
	R	-195	33	12	6/173
8 Passes	P	-206	30	10	27/185
	R	-204	28	10	1/177
Livingston		$E_{\text{corr}}$ [mV]	$i_{\text{corr}}$ [ $\mu\text{A}/\text{cm}^2$ ]	$i_{\text{an}}$ [ $\text{mA}/\text{cm}^2$ ]	$E_{\text{p1}}/E_{\text{p2}}/E_{\text{p3}}$ [mV]
0 Pass	P	-234	52	10	-38/166/236
	R	-185	243	12	-47/161/199
8 Passes	P	-244	44	13	-42/156/262
	R	-183	318	10	-53/175

### 3.2.1 The effect of deformation

Figure 4 shows an example of a typical potentiodynamic polarization curve of the CG (0 Pass) and UFG (8 Passes) copper measured in 1M HCl electrolyte (pH = 0.16) at room temperature. Both specimens exhibit a similar polarization behaviour with three active-passive transitions. The only difference is that the steady state anodic current is achieved in the specimen after 8 passes whereas in the CG specimen the current density continues to increase after the third passivation. A similar behaviour was also observed in 3% NaCl and in Livingston solution (not shown here). The individual electrochemical characteristics as determined from the potentiodynamic curves in all three solutions are summarized in Table 1 (where an asterisk signifies that steady state current density was not achieved in the measured range and the value in the Table corresponds to the current density at 800 mV<sub>SCE</sub>). All quantities given in the Table are indicated on the curves in Fig. 4.

### 3.2.2 The influence of surface quality

In order to estimate the influence of the quality of the surface on the corrosion behaviour, two types of samples were investigated. The sample with a “rough” surface was prepared only by mechanical polishing on fine emery papers (marked ‘R’ in the Table), while the sample with a polished surface (marked ‘P’) was electrolytically polished in H<sub>3</sub>PO<sub>4</sub> with ethanol solution. The polarization curves for the UFG material with these two surface qualities measured in 1M HCl solution

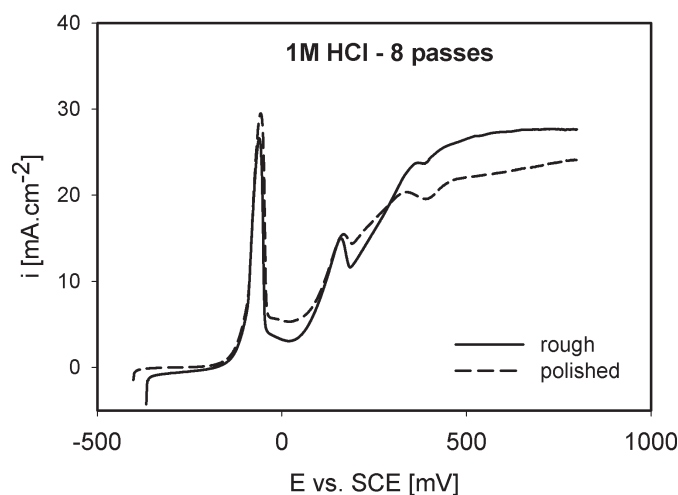


Fig. 5. Potentiodynamic polarization curve of the UFG specimen with rough and polished surface measured in 1M HCl.

are shown in Fig. 5. From the thermodynamics viewpoint the corrosion resistance of the specimen with the polished surface is lower ( $-275$  mV) than that of the specimen with the rough surface ( $-183$  mV). However, the corrosion rate for the specimen with the polished surface is much lower. The anodic dissolution rate (as characterized by the value of  $i_{an}$ ) was found to be approximately the same for the two surface conditions. The values of  $i_{an}$  in both specimens are similar within the experimental scatter. (Note that five potentiodynamic curves were measured for each state.) The individual active-passive transition regions are independent of the quality of the specimen surface. Strong dependence of corrosion rate on the surface quality was also found in Livingston solution both for UFG and CG specimen. In the case of NaCl solution, the corrosion rate was found to be independent of the quality of the surface.

### 3.2.3 The influence of pH

The potentiodynamic curve measured in two solutions with  $\text{Cl}^-$  ions differing in pH is shown in Fig. 6. The fine-grained specimen after 8 passes of ECAP with polished surface was chosen as an example and its behaviour in the standard Livingston solution is presented for comparison. The behaviour of a coarse grained Cu in these three solutions as well as of the CG and UFG Cu with mechanically polished surfaces is qualitatively the same, cf. the principal corrosion characteristics of all these measurements given in Table 1. The effect of pH on corrosion

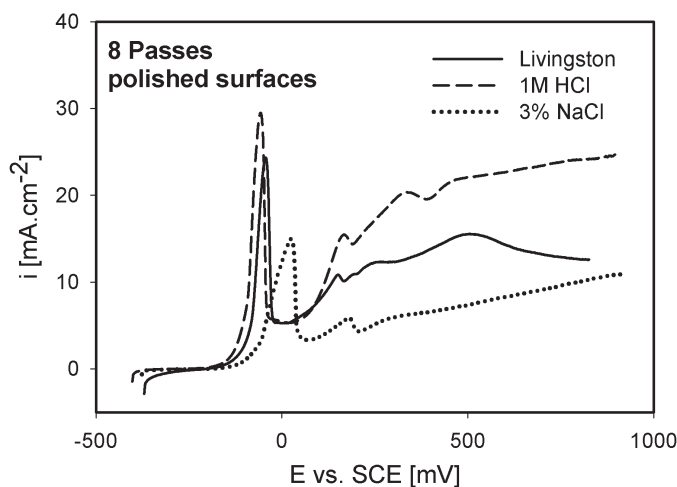


Fig. 6. Potentiodynamic polarization curves of the UFG Cu specimen in various aggressive media.

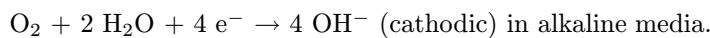
behaviour is shown in Fig. 6. The corrosion potential in HCl (pH = 0.16) is seen to be lower than in NaCl (pH = 7.01) indicating that the corrosion resistance of Cu increases with increasing pH of the aggressive solution.  $E_{\text{corr}}$  in Livingston solution (pH = 0.46) and in HCl differ only within the scatter of experimental data, while the corrosion rate seems to be independent of the test solution. The dissolution rate as characterized by the steady state anodic current is slightly higher in more acidic HCl than in neutral NaCl. Two active-passive transitions were observed in NaCl, while in HCl another transition at a high potential (350 mV<sub>SCE</sub>) is apparent. The overall corrosion behaviour of UFG Cu in Livingston solution is in good agreement with the results of Vinogradov [19] who measured corrosion properties during anodic polarization of commercial purity UFG Cu.

#### 4. Discussion

Microstructure evolution with the number of ECAP passes was discussed in the foregoing section. Here we will concentrate on the discussion of corrosion properties of UFG and CG Cu during anodic polarization in Cl<sup>-</sup> ion electrolytes focusing mainly on the influence of the concentration of Cl<sup>-</sup> ions (NaCl *vs.* HCl solutions), the pH value of the solution and the quality of the specimen surface (rough *vs.* polished surface) on possible primary reactions during the anodic polarization.

##### 4.1 Transition from the immune to active state – $E_{\text{corr}}$

In the cathodic region ( $E < E_{\text{corr}}$ ) a specimen behaves as a cathode and its surface is immune against corrosion. Any surface films which may have formed on the specimen are removed. Once the potential reaches the value of the corrosion potential  $E_{\text{corr}}$ , the specimen starts to get anodically polarized. Complicated processes including surface layer formation, their dissolution, transitions from the active to passive state may occur on the specimen surface. These processes, which are accompanied by mass transfer between the specimen and the electrolyte, influence the current density and its changes in the polarization circuit. The anodic polarization process starts at the potential  $E_{\text{corr}}$  at which the anodic and cathodic currents are in equilibrium. According to Deslouis [20] the kinetics and the mechanisms of anodic dissolution of copper in chloride solutions may be described by the following partial reactions:



According to  $E$ -pH diagrams [21] for Cu-Cl-H<sub>2</sub>O system, the increasing Cl<sup>-</sup> concentration extends the range of CuCl<sub>2</sub><sup>-</sup> stability towards more negative potentials. This is in accord with our measurements.  $E_{\text{corr}}$  in HCl (higher concentration

of  $\text{Cl}^-$  ions) is smaller (more negative) than in NaCl (smaller concentration of  $\text{Cl}^-$  ions), cf. Table 1. The value of  $E_{\text{corr}}$  is influenced by the concentration of  $\text{Cl}^-$  ions in the solution. In HCl with its higher concentration of these ions than in NaCl,  $E_{\text{corr}}$  is shifted to higher (negative) values, cf. Table 1.

## 4.2 Anodic corrosion behaviour

### 4.2.1 Polarization curve in 3% NaCl

Two distinct active-passive transitions were observed. According to the  $E$ -pH diagram [21], the first peak corresponds to the formation of CuO. The potential of CuO formation in neutral NaCl solution is approximately 20 mV<sub>SCE</sub>, which is in good agreement with measured transition potential  $E_{\text{p1}}$  in all samples (0 pass P/R surface, 8 passes P/R surface), cf. Table 1. With increasing potential the CuO layer is probably transformed into  $\text{Cu}_2\text{O}_3$ , which is manifested by the second peak on the anodic curve. This reaction is described in detail in the review paper [16]. The passive layer of  $\text{Cu}_2\text{O}_3$  remains stable with increasing potential and the corresponding current density tends to saturate at large values of potential.

### 4.2.2 Polarization curve in 1M HCl

Unlike in 3% NaCl, three active-passive transitions were found in 1M HCl. The main peak of the polarization curve was found at the potential of approximately  $-55$  mV<sub>SCE</sub>. It is associated with the cuprous oxide  $\text{Cu}_2\text{O}$  film formation on the specimen surface. Ives [15] and Leckie [16] reported the formation of this layer in coarse grained copper immersed into sulphuric acid and alkaline solution at about the same potential. The second active-passive transition corresponds to the formation of  $\text{Cu}_2\text{O}_3$ , as this layer is formed approximately in the same potential range as in 3% NaCl. The last peak on the curve may be ascribed to the formation of a CuCl layer. According to  $E$ -pH diagrams [21], such a layer may be formed only at a higher potential around 350 mV<sub>SCE</sub>. King [21] reported this layer to be stable at  $\text{Cl}^-$  concentrations exceeding 0.5 M. That is why this transition was not observed in 3% NaCl. With further increase of  $E$  the current density saturates. However, the steady state anodic current density is higher than in 3% NaCl, which indicates an enhanced dissolution rate of Cu in 1M HCl than in 3% NaCl. This difference is caused by different concentration of  $\text{Cl}^-$  ions and pH values in these two solutions as documented by plots of the dependence of the solubility of  $\text{Cu}_2\text{O}$  on pH and Cl concentration in [21].

## 4.3 The influence of the surface quality on the corrosion behaviour

The surface quality affects some corrosion properties of coarse grained and UFG copper. The corrosion resistance of electropolished specimen is lower than that

of mechanically polished specimen. Electrochemical processes during electropolishing increase the reactivity of the surface which is thermodynamically less resistant to corrosion attack than mechanically polished surface. On the other hand, the corrosion rate (characterized by  $i_{\text{corr}}$ ) of the specimens with smoothly electropolished surface is significantly lower than that of specimens with rough, mechanically polished, surface. This difference is partly caused by geometrical factors, as the active area of a rough surface exposed to the corrosion attack is effectively larger than the area of a smooth surface. Also, asperities on a rougher surface lead to locally increased electric field. Furthermore, corrosion products adhere to a smooth surface much better than to a rough surface. Such a layer is more compact and less porous. From the kinetics viewpoint, a smooth surface is therefore more corrosion resistant than a rough one. After active-passive transition the influence of the initial surface is less pronounced and the difference in corrosion characteristics at higher values of potential and in the transpassive region diminishes ( $i_{\text{an}}$  and  $E_{\text{pn}}$  of mechanically polished and electropolished specimens differing within the experimental scatter only).

#### 4.4 Morphology of corrosion damage

The corrosion properties evaluated from potentiodynamic measurements cannot completely characterize the corrosion behaviour of polycrystalline materials. Another important aspect is localization of corrosion degradation. In order to characterize the overall resistance against environmental attack, it is necessary to evaluate the degree of localization of corrosion damage [22]. In our previous work [23] we studied the morphology of specimen surface after potentiodynamic polarization using scanning electron microscopy. It was found that ultra-fine grained copper after ECAP corroded significantly more uniformly than coarse grained copper, which showed localized intergranular corrosion. Hence, in this sense, extreme grain refinement by ECAP affects the corrosion properties in a positive way.

### 5. Conclusions

Microstructure evolution of ultra-fine grained copper produced by equal channel angular pressing was investigated by transmission electron microscopy. The corrosion behaviour was evaluated by potentiodynamic polarization measurements in neutral 3% NaCl and acidic 1M HCl solutions.

– TEM analysis showed that the microstructure evolves from a lamellar grain arrangement (1 pass) through elongated dislocation cells and/or subgrains (4 passes) to an equiaxed homogeneous grain structure (8 passes). With increasing strain the misorientation between cells/subgrains increases, while the dislocation cell size of 200–500 nm established after the first pass remains nearly unchanged.

– Grain refinement by ECAP does not qualitatively change the general electrochemical characteristics of Cu.

– Corrosion damage was found to be homogeneous in the ultra-fine grained material, as distinct from the clearly localized intergranular corrosion in coarse grained material.

– The surface quality, the pH value and the concentration of  $\text{Cl}^-$  ions in the solutions influence some electrochemical characteristics of coarse grained and ultra-fine grained copper significantly. In particular,

– from the thermodynamic viewpoint an electropolished surface is less corrosion resistant than a mechanically polished surface,

– from the kinetics viewpoint an electropolished surface corrodes slower than a mechanically polished surface in more acid solutions,

– lower pH values and higher  $\text{Cl}^-$  concentration in the solution raise the dissolution rates of the material in the transpassive region (at large values of the potential).

### Acknowledgements

The authors would like to dedicate this paper to Prof. RNDr. Pavel Lukáč, DrSc., Dr.h.c. on the occasion of his 70<sup>th</sup> birthday.

This work was supported by GACR under grant 106/05/2347, by the State Program of the Slovak Republic “New materials and technologies in machine and equipment construction”, the Slovak-Czech cooperation project (Kontakt) No. 093/2004 (M. J., B. H.) and by DFG under grant Es 74/13 (Y. E. and R. H.).

### REFERENCES

- [1] MINGLER, B.—KARNTHALER, H. P.—ZEHETBAUER, M.—VALIEV, R. Z.: *Mat. Sci. Eng.*, A319–321, 2001, p. 242.
- [2] MISHIN, O. V.—JUUL JENSEN, D.—HANSEN, N.: *Mat. Sci. Eng.*, A342, 2003, p. 320.
- [3] DALLA TORRE, F. H.—LAPOVOK, R.—SANDLIN, J.—THOMSON, P. F.—DAVIES, C. H. J.—PERELOMA, E. V.: *Acta Mater.*, 52, 2004, p. 4819.
- [4] LIAN, J.—VALIEV, R. Z.—BAUDELET, B.: *Acta Metall.*, 43, 1995, p. 4165.
- [5] HELLMIG, R. J.—BAIK, S. C.—SEO, M. H.—KIM, S. H.—ESTRIN, Y.: *Vop. Mater.*, 33, 2003, p. 168.
- [6] XU, C.—FURUKAWA, M.—HORITA, Z.—LANGDON, T. G.: *Jour. of Alloys and Compounds*, 378, 2004, p. 27.
- [7] SIOW, K. S.—TAY, A. A. O.—ORUGANTI, P.: *Mat. Sci. Tech.*, 20, 2004, p. 285.
- [8] SANDERS, P. G.—EASTMAN, J. A.—WEERTMAN, J. R.: *Acta Mater.*, 45, 1997, p. 4019.
- [9] AGNEW, S. R.—WEERTMAN, J. R.: *Mater. Sci. Eng.*, A244, 1998, p. 145.
- [10] SANDERS, P. G.—RITTNER, M.—KIEDAISH, E.—WEERTMAN, J. R.—KUNG, H.—LU, Y. C.: *Nanostr. Mater.*, 9, 1997, p. 433.
- [11] ESTRIN, Y.—TÓTH, L. S.—MOLNIARI, A.—BRÉCHET, Y.: *Acta Mater.*, 46, 1998, p. 5509.
- [12] BAIK, S. C.—ESTRIN, Y.—KIM, H. S.—HELLMIG, R. J.: *Mat. Sci. Eng.*, A351, 2003, p. 86.
- [13] AUST, K. T.—ERB, U.—PALUMBO, G.: *Mater. Sci. Eng.*, A176, 1994, p. 329.

- 
- [14] ROFAGHA, R.—ERB, U.—OSTANDER, D.—PALUMBO, G.—AUST, K. T.: Nanostr. Mater., 2, 1993, p. 1.
- [15] IVES, D. J. G.—RAWSON, A. E.: J. Electrochem. Soc., 109, 1962, p. 447.
- [16] LECKIE, H. P.: J. Electrochem. Soc., 117, 1970, p. 1478.
- [17] HADZIMA, B.—PALČEK, P.—CHALUPOVÁ, M.—ČANÁDY, R.: Kovove Mater., 41, 2003, p. 257.
- [18] HUGHES, D. A.—HANSEN, N.: Acta Mater., 45, 1997, p. 3871.
- [19] VINOGRADOV, A.—MIMAKI, T.—HASHIMOTO, S.—VALIEV, R.: Scripta Mater., 41, 1999, p. 319.
- [20] DESLOUIS, C.—TRIBOLLET, B.—MENGOLI, G.—MUSIANI, M.: Jour. Appl. Electrochemistry, 18, 1998, p. 374.
- [21] KING, F.: Corrosion of copper in alkaline chloride environments. Tech. Report TR-02-25, SKB, Stockholm 2002.
- [22] PALČEK, P.—CHALUPOVÁ, M.—NICOLETTO, G.—BOKŮVKA, O.: Prediction of Machine Element Durability. Žilina, University of Žilina 2003.
- [23] HADZIMA, B.—JANEČEK, M.—HELLMIG, R. J.—KUTNYAKOVA, Y.—ESTRIN, Y.: Mat. Sci. Forum, 2005 (in press).